

Development of a bone reconstruction technique using a solid free-form fabrication (SFF)-based drug releasing scaffold and adipose-derived stem cells

Jin Woo Lee,^{1*} Ki-Joo Kim,^{2*} Kyung Shin Kang,³ Shaochen Chen,^{1,4} Jong-Won Rhie,² Dong-Woo Cho^{3,5}

¹Department of NanoEngineering, The University of California, San Diego, La Jolla, California 92093-0448

²Department of Plastic Surgery, School of Medicine, The Catholic University of Korea, Seoul 137-701, Republic of Korea

³Department of Mechanical Engineering, Pohang University of Science and Technology (POSTECH), San 31, Hyoja-dong, Nam-gu, Pohang, Gyungbuk, 790-784, Republic of Korea

⁴Institute of Engineering in Medicine, The University of California, San Diego, La Jolla, California 92093-0448

⁵Division of Integrative Biosciences and Biotechnology, Pohang University of Science and Technology (POSTECH), San 31, Hyoja-dong, Nam-gu, Pohang, Gyungbuk, 790-784, Republic of Korea

Received 7 April 2012; revised 8 October 2012; accepted 9 October 2012

Published online 27 November 2012 in Wiley Online Library (wileyonlinelibrary.com). DOI: 10.1002/jbm.a.34485

Abstract: For tissue regeneration, three essential components of scaffolds, signals (biomolecules), and cells are required. Moreover, because bony defects are three-dimensional in many clinical circumstances, an exact 3D scaffold is important. Therefore, we proposed an effective reconstruction tool for cranial defects using human adipose-derived stem cells (hADSCs) and a 3D functional scaffold fabricated by solid free-form fabrication (SFF) technology that secretes biomolecules. We fabricated poly(propylene fumarate)-based 3D scaffolds with embedded microsphere-deliverable bone morphogenetic protein-2 (BMP-2) by microstereolithography. BMP-2-loaded SFF scaffolds with/without hADSCs (SFF/BMP/hADSCs scaffolds and SFF/BMP scaffolds, respectively) and BMP-2-unloaded SFF scaffolds (SFF scaffolds) were then implanted in rat crania, and *in vivo* bone formation was observed. Analyses

of bone formation areas using micro-computed tomography (micro-CT) showed the superiority of SFF/BMP/hADSCs scaffolds. Hematoxylin and eosin stain, Masson's trichrome stain, and collagen type-I stain supported the results of the micro-CT scan. And human leukocyte antigen-ABC showed that seeded, differentiated hADSCs were well grown and changed to the bone tissue at the inside of the scaffold. Results showed that our combination of a functional 3D scaffold and hADSCs may be a useful tool for improving the reconstruction quality of severe bony defects in which thick bone is required. © 2012 Wiley Periodicals, Inc. *J Biomed Mater Res Part A*: 101A: 1865–1875, 2013.

Key Words: bone-tissue engineering, scaffold, bone morphogenetic protein (BMP), human adipose-derived stem cells (hADSCs), solid free-form fabrication (SFF)

How to cite this article: Lee JW, Kim K-J, Kang KS, Chen S, Rhie J-W, Cho D-W. 2013. Development of a bone reconstruction technique using a solid free-form fabrication (SFF)-based drug releasing scaffold and adipose-derived stem cells. *J Biomed Mater Res Part A* 2013;101A:1865–1875.

INTRODUCTION

Tissue engineering recovers a tissue's original function by substituting the damaged part of the human body with a new tissue or organ regenerated by various technologies. This technology utilizes three essential components: scaffolds, signals (biomolecules), and cells. When these components are suitably combined, the best regeneration results can be acquired.

Stem cells, the first essential component of tissue engineering, are a group of undifferentiated cells that have the capacity to self-renew and generate differentiated cells.

Tissue engineering using stem cell technology has shown great promise for future regenerative medicine. Thus far, various stem cells, including embryonic stem cells (ESCs), bone marrow stem cells (BMSCs), mesenchymal stem cells (MSCs), and adipose-derived stem cells (ADSCs), have been reported. These stem cells have been widely utilized to reconstruct damaged tissues and organs.^{1,2} However, some types of stem cells have limitations. For example, ESCs have not been free from ethical criticism. Furthermore, although research using BMSCs has been performed for a long time and numerous cases of positive results have reported, the

Additional Supporting Information may be found in the online version of this article.

*These authors contributed equally to this work.

Correspondence to: Professor D-W Cho; e-mail: dwcho@postech.ac.kr or J-W Rhie; e-mail: rhie@catholic.ac.kr

Contract grant sponsor: National Research Foundation of Korea (NRF) grant by the Korea Government (MEST); contract grant number: 2012-0001235

supply of cells has not been sufficient until now. However, because ADSCs can be harvested from the adipose tissue of an adult, thereby avoiding the ethical dispute,³⁻⁶ ADSCs have attracted a great deal of attention. When ADSCs were compared with BMSCs, it was reported that a comparatively large amount of ADSCs could be extracted from adipose tissue (500 times the amount derived from bone marrow).⁷ Moreover, because of the increased adipose tissue removal in obese patients, a sufficient supply of ADSCs can be guaranteed. Thus, especially with regard to a stable supply, ADSCs may be the most advantageous candidate among the various stem cells.

Meanwhile, cell-suspension injections do not seem to be suitable for large tissue reconstruction.^{8,9} Therefore, scaffolds are also required to reconstruct the tissue or organ. To date, most scaffolds in tissue engineering have been fabricated by conventional fabrication methods,¹⁰⁻¹⁷ including particulate leaching and phase separation/inversion. However, fabrication of adapted scaffolds is problematic due to considerations of cell growth and tissue regeneration because control of the internal or external architecture is difficult using these methods. Many studies have recently been performed seeking to overcome these disadvantages of conventional fabrication methods and offer other options. One such option is solid free-form fabrication (SFF) technology using computer-aided design (CAD) and computer-aided manufacturing (CAM). Various SFF technologies,¹⁸⁻³⁰ such as microstereolithography (MSTL) and three-dimensional printing (3DP), have been developed. Among them, MSTL is a technology that allows comparatively high throughput and high resolution.

Biomolecules, such as growth factor, stimulate tissue regeneration *in vitro* and *in vivo*. In particular, bone morphogenetic protein-2 (BMP-2), a family of proteins that are members of the transforming growth factor-beta (TGF- β) superfamily, has a stimulating effect on bone formation in orthopedic applications. However, despite its strong osteoinductive activity, the lack of a suitable delivery system has limited the clinical use of BMP-2. Although microspheres have attracted attention as a delivery system for BMP,³¹⁻³⁷ they do not perform the scaffold functions of load bearing or providing living space for cells because of their low mechanical properties and limited architecture fabrication.

Thus, in this study, considering the three essential components, we proposed a new tool to reconstruct cranial defects using SFF-based 3D functional scaffolds that release biomolecules and use hADSCs as a cell source. Namely, we fabricated 3D scaffolds with embedded microspheres-deliverable BMP-2 by MSTL using a mixture of microspheres and biodegradable photopolymer. Fabricated scaffolds were implanted into rat calvaria, and *in vivo* bone formation was observed. By measuring bone formation areas using microcomputed tomography (micro-CT) and various histological assays, we observed the effect of the scaffold and the released BMP-2 and hADSCs.

MATERIALS AND METHODS

Synthesis of the photopolymer

PPF was synthesized by a condensation reaction as described elsewhere.²⁸ Briefly, 2.4 mol fumaric acid (Sigma-

Aldrich, St. Louis, MO) and 3.0 mol propylene glycol (Kanto Chemical, Tokyo, Japan) were placed in a triple-necked flask with an overhead electrical stirrer for synthesis. During synthesis, the temperature of the solution was increased from room temperature to 180°C. The reaction was ended after 18 h, and the final product was a clear, light yellow, very viscous liquid. To use PPF as a liquid polymer for MSTL, diethyl fumarate (DEF) (Tokyo Kasei Kogyo, Tokyo, Japan) as a low-viscosity cross-linking agent was added in a 70:30 ratio (PPF to DEF). The photo-initiator I2959 (Ciba, Tokyo, Japan) was then added at 1% (w/w) and dissolved thoroughly.

Fabrication of growth factor-loaded microspheres

Microspheres were produced using poly(lactic-co-glycolic acid) (PLGA) and deionized water as described elsewhere.²⁸ Briefly, microspheres were fabricated from PLGA in a 50:50 lactic to glycolic acid ratio and MW of 40,000–75,000 in a double-emulsion process. PLGA (0.2 g) was dissolved in 2 mL of dichloromethane (99.8%, Sigma-Aldrich, St. Louis, MO), and the dissolved solution was agitated at constant speed in a vortex mixer (Vortex Genie 2; Scientific Industries, Bohemia, NY). After 10 μ g of recombinant human BMP-2 (rhBMP-2) (Peprotech, Rocky Hill, NJ) was dissolved in deionized water, an aqueous BMP-2 solution was mixed with the PLGA solution and swirled for 2 min using a homogenizer (Ultra-Turrax T18; IKA, Staufen, Germany). Immediately following the preparation of this emulsion, 20 mL of 0.5% polyvinylalcohol (PVA) (87–89% hydrolyzed, MW of 31,000–50,000; Sigma-Aldrich) was added to serve as a surfactant, and the mixture was swirled at a homogenizing speed of 8000 rpm for 2.5 min. After the second emulsifying process, the contents were poured into a 2% isopropyl alcohol (IPA; Mallinckrodt Baker, Phillipsburg, NJ) aqueous solution maintained on a magnetic stirrer. This mixture was stirred for 3 h under a chemical hood. The organic phase solvent, dichloromethane, was evaporated during that time. Microspheres were then gathered from the IPA solution using a centrifuging machine, dried in a –90°C freeze-dryer for 1 day, and stored at –20°C.

Scaffold fabrication method using MSTL

MSTL was used to fabricate free-form 3D microstructures by dividing a desired shape into slices of a given thickness. During MSTL, an ultraviolet (UV) laser irradiates the free surface of a UV-curable liquid photopolymer, causing it to solidify. A focused laser beam of a few micrometers in diameter is used to solidify a very small area of liquid photopolymer. A heating device was installed at the bottom of the reservoir to decrease the viscosity of the photopolymer. To fabricate the scaffold, a continuous-wave diode laser ($\lambda = 375$ nm, radius 375; Coherent, Santa Clara, CA) and an x-y-z stage (ATS-100; Aerotech, Pittsburgh, PA) with 500-nm resolution were used. Figure 1 shows a schematic diagram (A) and photograph of the installed MSTL system (B).

Cell isolation and cultivation

Human subcutaneous lipoaspirates were collected from patients after obtaining informed written consent. The tissues were washed at least three times with a phosphate-

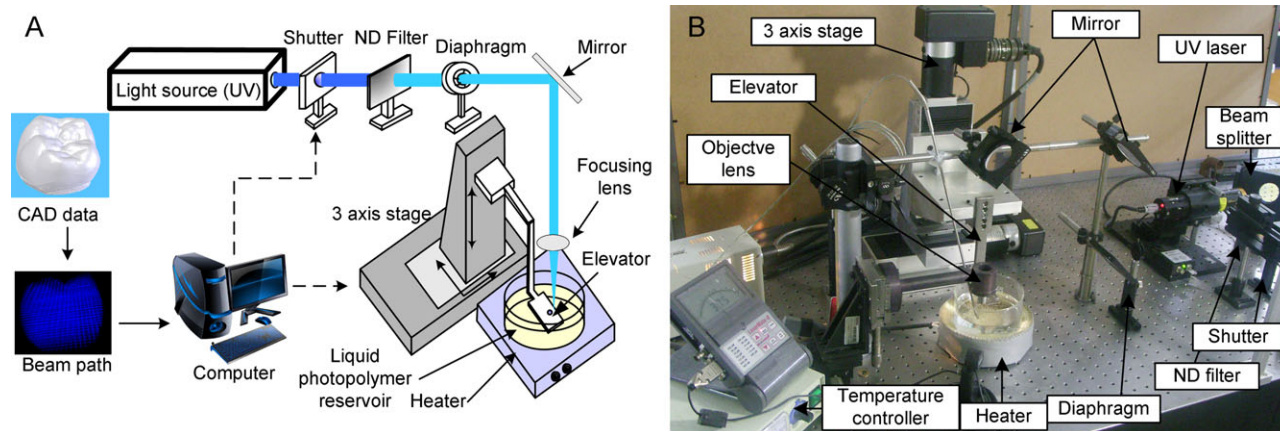


FIGURE 1. Schematic illustration (A) and setup of the microstereolithography system (B). [Color figure can be viewed in the online issue, which is available at wileyonlinelibrary.com.]

buffered saline (Sigma-Aldrich) solution to remove contaminating debris and blood. The tissue was then digested with 0.05% type-I collagenase (Sigma-Aldrich) in the phosphate-buffered saline solution for 30 min at 37°C with gentle agitation. After filtration through a 100- μ m mesh filter and subsequent centrifugation, adipocytes and hematopoietic stem cells were removed from the stromal-vascular fraction. The isolated hADSCs in the stromal-vascular fraction were cultured in Dulbecco's modified Eagle's medium (DMEM; Gibco, Grand Island, NY) supplemented with 10% (v/v) fetal bovine serum (FBS; Gibco), 100 U/mL penicillin (Gibco), and 0.1 mg/mL streptomycin (Gibco) in humidified air with 5% (v/v) CO₂ at 37°C. The cells were cultured for three passages.

Cell seeding and proliferation

After sterilization with ethylene oxide, the scaffolds were aired out under a fume hood for 1 day and then soaked in DMEM supplemented with 10% FBS for 1 day. The medium was removed for cell seeding, and 2×10^5 hADSCs-derived osteoblasts, which were evaluated in our previous research,²⁹ in 50 μ L of osteogenic media were seeded onto the scaffolds. The scaffolds were kept in the medium for 2 days before implantation.

In vivo implantation

We conducted an *in vivo* implantation experiment following the animal care guidelines of the National Institutes of Health and the Catholic University Medical College Institutional Animal Care Committee. Wistar rats (12-week-old males, average weight 350–400 g) were used. Routine antibiotics and analgesics were prescribed preoperatively to prevent infection and reduce pain during and after the operation, and general anesthesia was induced with a combination of ketamine (Yuhan Co., Seoul, Korea) and Xyloraine (2:1 ratio, 2.5 mL/kg). The dorsal scalp of each rat was shaved and disinfected with a routine antiseptic solution. A local anesthetic (1% lidocaine with epinephrine 1:100,000) was injected for hemostasis and to increase tissue bulk. A medial sagittal incision was made using a no.

15 blade, and the overlying tissue was dissected to expose the cranial bone.³⁸ A full-thickness bony defect was created in the central part of the cranial bone using a hollow trephine bur with an 8-mm outer diameter. During the operation, extreme care was taken to minimize damage to the dura mater, and any animals showing evident injuries in the meninges or continuous hemorrhaging were excluded from the experiment. BMP-2-loaded SFF scaffolds and BMP-2-unloaded SFF scaffolds produced using MSTL were then placed in the 8-mm cranial defects. BMP-2-unloaded SFF scaffolds (PPF scaffolds) were used as negative controls. Two groups of BMP-2-loaded SFF scaffolds (PPF/BMP scaffolds and PPF/BMP/hADSCs scaffolds) were prepared, and hADSCs were seeded in one group (PPF/BMP/hADSCs scaffold). Thus, the experiment comprised three groups: PPF scaffolds, PPF/BMP scaffolds, and PPF/BMP/hADSCs scaffolds. Each experimental group consisted of four rats. After inserting the scaffolds, 4–0 nylon sutures were used to close the pericranium and the overlying skin. For immunosuppression, the animals were given intraperitoneal cyclosporine A (CSA, 10 mg/kg body weight; Novartis Korea, Seoul, Korea) for 11 weeks.

Fixation of the samples

After decalcification, samples were embedded in paraffin, and a paraffin form was made. Decalcification solution was prepared by mixing 100 g of EDTA, 6 g of NaOH, and 12.1 g of Tris with 1 L of distilled (DI) water; the pH level was maintained at 7.4. The decalcification solution was changed every 3 days for 4 weeks. After decalcification, samples were put in the cubic reservoir, and a paraffin was filled. The paraffin block was sliced into 4- μ m thicknesses, and each slice was stained.

Morphology

The morphology of the scaffold was examined using scanning electron microscopy (SEM) (JSM-6390LV, JEOL, Tokyo, Japan) at 1–15 kV. All samples were coated with gold using a sputter coater (Sputter Coater 108 auto, Cressington Scientific, Watford, UK) for 40 s.

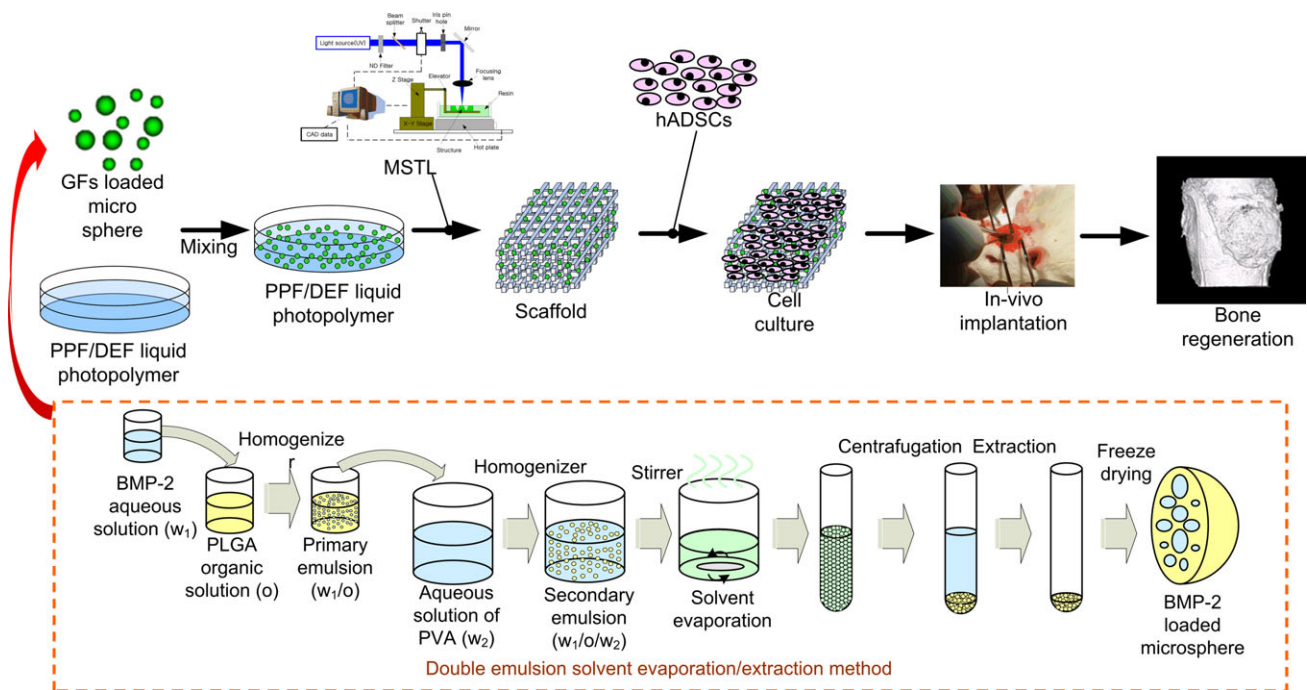


FIGURE 2. Schematic illustration of the scaffold fabrication procedure using microstereolithography and the double-emulsion process to fabricate BMP-2-loaded microspheres. [Color figure can be viewed in the online issue, which is available at wileyonlinelibrary.com.]

Analysis of *in vivo* experiment results

Four rats per experimental group were sacrificed by CO₂ inhalation 11 weeks after surgery, and the degree of bone formation was examined using micro-CT (Dr. Gem, Seoul, Korea). After visualization of the bone healing by micro-CT scanning, the samples were embedded in paraffin, and tissues were sectioned at 4 μm. Histological analysis was performed following hematoxylin and eosin stain, Masson's trichrome stain, and immunohistochemistry-paraffin stain (collagen type-I and HLA-ABC). Sections were then observed under an optical microscope (AX70, TR-62A02, Olympus, Tokyo, Japan).

Bone mineral density (BMD)

The parameters of bone mass and micro-architecture were evaluated using the built-in software of micro-CT (Dr. Gem, Seoul, Korea). BMD was calibrated by means of phantoms [calcium hydroxyapatite (CaHA): 0.75g/cm³ and 0.25g/cm³] with known BMD.

Hematoxylin and eosin stain

After deparaffinization, slices were kept in hematoxylin for 5 min, washed with DI water, and dipped into 1% acid alcohol (HCl + 70% EtOH) for 10 s. After washing with DI water, the slice was dipped into eosin (HX073987, Merck KGaA, Darmstadt, Germany) for 3 min, washed with DI water, and dipped into ammonia for 10 s. Next, they were washed with DI water again and dehydrated using 70%, 80%, 90%, and 100% ethanol and xylene.

Masson's trichrome stain

After deparaffinization, the sample slices were dipped into Bouin's solution (HT10132-1L, Sigma) and kept for 30 min

at 56°C. Each of them were then washed thoroughly with streaming water for 10 min and dipped into scarlet solution (B6008-25G, Sigma), phosphomolybdic-phosphotungstic acid (phosphomolybdic acid, JUNSEI, Tokyo, Japan; phosphotungstic acid, JUNSEI), and aniline blue solution (M5528-25G, Sigma) for 10 min. Next, they were washed with DI water and dipped into acetic acid for 3 min and hematoxylin for 10 min. Finally, they were washed again with DI water and dehydrated.

Immunohistochemistry-paraffin (IHC-P) stain

After deparaffinization, the sample slices were dipped into 3% quenching endogenous peroxidase (9B3501, JUNSEI, Japan) and washed in DI water. They were then dipped into pH 6.0, 1× citrate buffer (18598, ScyTeK Laboratories, Logan, UT), kept for 5 min in a microwave and 20 min in an oven at 75°C, and then cooled at room temperature. After three washing cycles using DI water and TBS-T (Tris-Buffered Saline Tween-20), the samples were dipped into 2.5% normal horse serum (ABC kit, PK-6102, Vector, Loerach, Germany) for 20 min and then kept overnight at 4°C as the primary antibody became attached. In that process, collagen type-I antibody (ab6308, Abcam, Cambridge, MA) and human leukocyte antigen (HLA)-class 1 ABC antibody (ab70328, Abcam) were used. The samples were then treated with biotin-conjugated secondary antibody (ABC kit, PK-6102, Vector), avidin-Biotin complex (ABC kit, PK-6102, Vector), and 3,3'-diaminobenzidine (DAB) solution (SK-4100, Vector) for 60 min, 30 min, and 1 min, respectively. Before each treatment, the samples were washed by TBS-T. After treatment with the DAB solution, the samples were colorized. Colorized samples were washed with DI

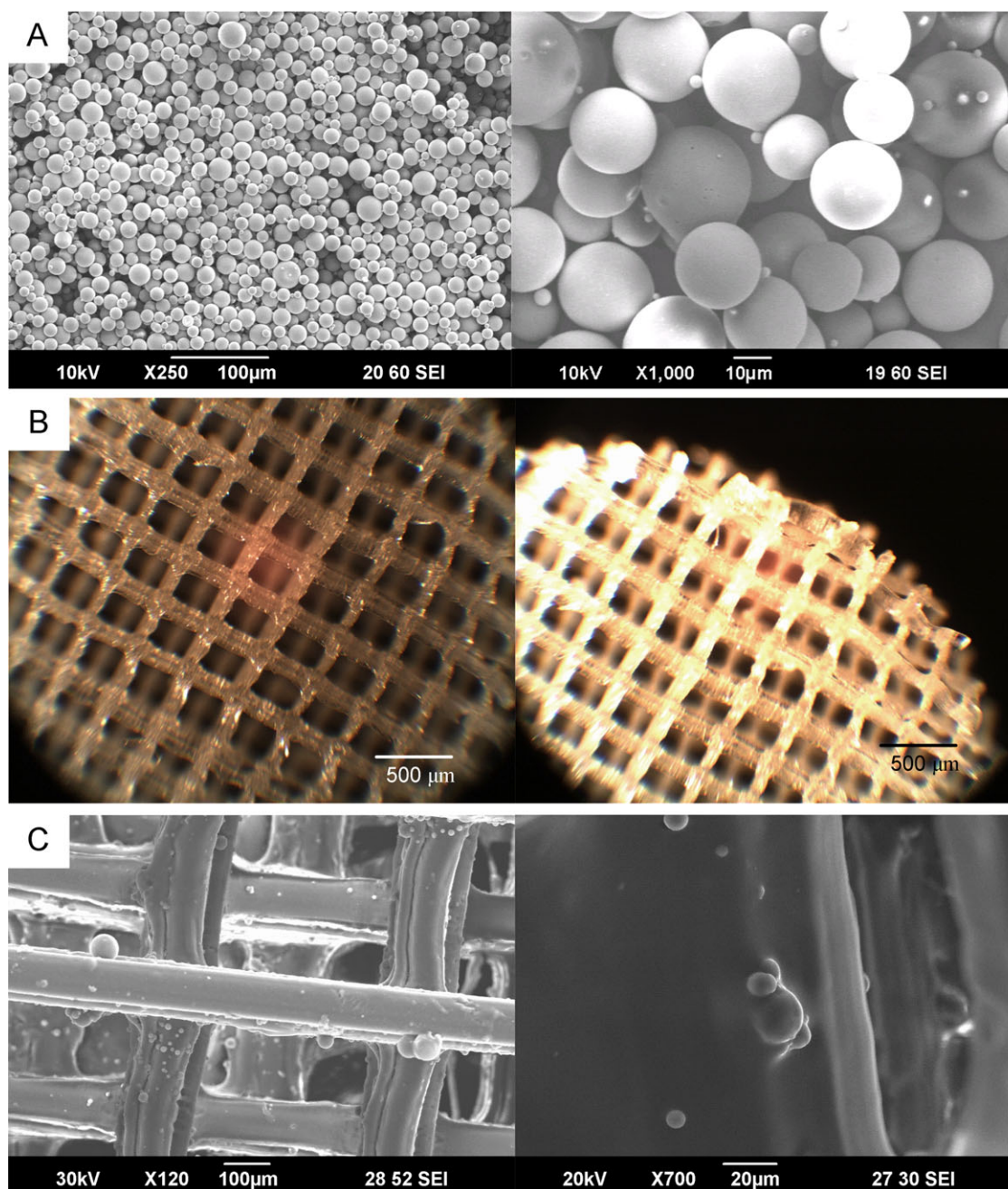


FIGURE 3. BMP-2-loaded 3D scaffold. (A) SEM images of the fabricated BMP-2-loaded microspheres, (B) microscopic images of the fabricated SFF scaffold, and (C) SEM images of the microspheres embedded 3D scaffold. [Color figure can be viewed in the online issue, which is available at wileyonlinelibrary.com.]

water and dipped into hematoxylin for 1 min. After adding ammonium water, the samples were dehydrated.

Statistical analysis

The results are expressed as the mean \pm standard deviation (SD). Statistical significance was determined by analysis of variance (ANOVA) using a software program (MINITAB version 14.2, Minitab, State College, PA). Statistical significance was accepted when $p < 0.05$.

RESULTS

Fabrication of the 3D BMP-2-loaded scaffold

The BMP-2-loaded scaffold was fabricated using BMP-2-loaded microspheres, PPF/DEF photopolymer, and the MSTL system (Fig. 2). The concentration of BMP-2-loaded microspheres was based on those reported by other researchers.^{39–41} To solidify the liquid suspension of BMP-2-loaded microspheres fabricated by a double-emulsion process [Fig. 3(A)] and PPF/DEF photopolymer, the selected laser scan speed and laser power were 60 mm/min and 280 mW,

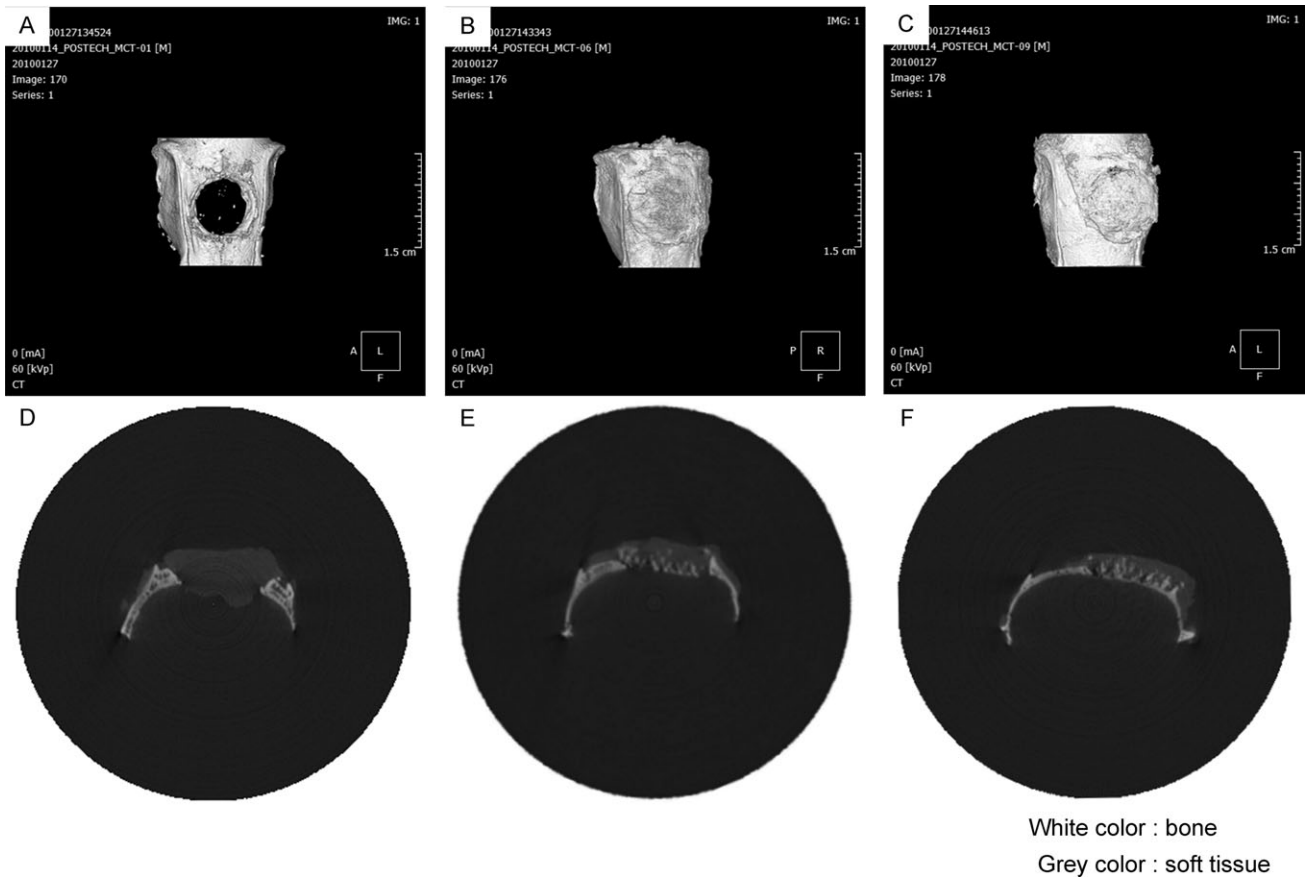


FIGURE 4. Micro-CT images of rat cranial bone at 11 weeks after implantation. (A) 3D reconstructed image of PPF scaffold (negative control), (B) 3D reconstructed image of PPF/BMP scaffold, (C) 3D reconstructed image of the PPF/BMP/hADSCs scaffold, (D) cross-sectional image of PPF scaffold (negative control), (E) cross-sectional image of PPF/BMP scaffold, and (F) cross-sectional image of PPF/BMP/hADSCs scaffold.

respectively. Under these conditions, we fabricated a 3D scaffold that consisted of a staggered arrangement of lines [Fig. 3(B)]; since two layers were stacked to fabricate the line structures and each layer was 200 μm thick, the final pore height was 400 μm . Finally, eight layers were stacked to give a scaffold height of 1600 μm and a thickness of 400 μm . Although the dimensions of the scaffold were decreased by shrinkage during the cleaning process, it kept its shape due to the symmetric quality of the shrinkage. The strut pitch and thickness of the final scaffold for implantation were 450 and 1200 μm , respectively. Its shrinkage rate was 25%. When we observed the fabricated scaffold, microspheres were well embedded on the scaffold without excessive conglomeration [Fig. 3(C)]. The average weight of the scaffold was 66 mg, and microspheres of 0.66 mg per scaffold (1 wt% of the scaffold weight) on average were embedded. Since BMP-2 was loaded to the PLGA microspheres in a ratio of 1:20,000, if no loss of BMP-2 occurs as a result of the double-emulsion process during microsphere fabrication, each scaffold should have contained 33-ng BMP-2.

***In vivo* bone-formation analysis**

In a previous study, we evaluated both the BMP-2 release profile in our 3D functional scaffold and pre-osteoblast

differentiation *in vitro*.²⁸ However, we did not investigate the correlation between BMP-2 and stem cells. Therefore, based on the ethical criticism and sufficiency of the supply, we chose the hADSCs among various stem cells in this study. To investigate the bone-formation performance of BMP-2 and hADSCs *in vivo*, three groups, the PPF scaffolds, PPF/BMP scaffolds, and PPF/BMP/hADSCs scaffolds groups, were prepared. The diameter and thickness of each scaffold were 8 and 1.2 mm, respectively. The prepared scaffolds were implanted into the 8-mm-diameter bony defect created in the central part of the rat cranial bone. To validate and visualize bone healing, a micro-CT scan was taken at week 11 after surgery. After 11 weeks, on the PPF/BMP/hADSCs scaffolds, newly formed bone of a clear white color was observed in the CT image; this color indicated the presence of a thick generated bone [Fig. 4(C)]. On the PPF/BMP scaffolds, although new bone was generated in most of the bony defect zone, the formed bone was thin [Fig. 4(B)]. Ectopic bone formation by BMP-2 release to the unintended location did not occur in either the PPF/BMP scaffold or PPF/BMP/hADSCs scaffold groups. The negative control group, the PPF scaffolds, demonstrated limited bone healing and only in the periphery of the defect [Fig. 4(A)]. As shown in Figure 4(D-F), cross-sectional views of the rat cranium

clearly showed the bone formation ability of each type of scaffold. On the PPF scaffolds, bone was not observed in the center area of the removed cranium. A comparison of results for PPF/BMP scaffolds and PPF/BMP/hADSCs scaffolds revealed that the area and thickness of bone formation were greater on PPF/BMP/hADSCs scaffolds than those on PPF/BMP scaffolds. In particular, marginal bone was linked with newly formed bone on the PPF/BMP/hADSCs scaffolds. When we analyzed the BMD of the formed bone, the BMDs of each group showed the same trends as those of the bone-formation areas. PPF scaffolds and PPF/BMP scaffolds exhibited densities of 0.440 and 0.556 g/cm³, respectively. In contrast, PPF/BMP/hADSCs scaffolds showed a density of 0.660 g/cm³. That is to say, BMP-2 and pre-osteoblast differentiation from ADSCs resulted in synergistic bone regeneration.

Hematoxylin and eosin stain results

The histological analysis using hematoxylin and eosin stain at week 11 after surgery revealed that a small amount of new bone had been generated from the margin of native bone, and ingrowth of cells was detected on PPF scaffolds [Fig. 5(A,B)]. However, on PPF/BMP scaffolds, owing to the secretion of BMP-2 at the outer surface of scaffold, ossified regions (new bone) had grown from the marginal bone toward the inside [Fig. 5(C, D)]. Multinucleated cells were produced around ossification areas. In particular, because ossification of penetrated cells was accelerated by the effect of BMP-2, we also observed large ossified areas on PPF/BMP/hADSCs scaffolds, and bone cores formed inside the scaffold were connected with one another [Fig. 5(E,F)].

Masson's trichrome stain results

With Masson's trichrome stain, collagen showing the occurrence of bone-tissue induction is stained blue, and calcified areas are stained red [Fig. 6(A–C)]. Our Masson's trichrome stain results were similar to the results of hematoxylin and eosin staining, namely PPF/BMP/hADSCs scaffolds-generated large ossified regions, as shown by hematoxylin and eosin staining. PPF/BMP scaffolds also showed ossified regions at the surroundings of the defect and several calcified spots at the center of the scaffold. Needless to say, the result of the PPF scaffolds was the least favorable. Since many collagens were generated by osteogenic stimulation by the BMP-2 that was secreted from the scaffold in the early stage of hADSCs differentiation, only PPF/BMP/hADSCs scaffolds showed several parts of the calcified areas stained blue to red [Fig. 6(C)].

Collagen type-I stain results

Collagen type-I stain images indicated results similar to those of Masson's trichrome stain. These images specifically showed the areas of regenerated bone. In the stained images, the areas composed of bone and fibrous tissues were stained brown, and we could distinguish differentiated zones by observing the congregation of many nuclei. Bone-formation areas were stained light blue, and nuclei were also observed in the stained areas. The scaffold was stained

blue. PPF/BMP/hADSCs scaffolds generated the largest areas of ossification, and PPF/BMP scaffolds also showed progressive ossification [Fig. 6(E,F)]. Small areas of bone formation were detected on PPF scaffolds [Fig. 6(D)]. Moreover, on PPF/BMP/hADSCs scaffolds, the distribution of collagen type-I showed that bone formation had progressed over the entire scaffold, including both the exterior and interior.

HLA-ABC stain results

To verify the effect of hADSCs on bone generation, we observed human leukocyte antigen-ABC (HLA-ABC), a human-tissue-specific marker. HLA-ABC was observed by identifying stained nuclei and cytoplasm around nuclei of brown color. The brown-stained tissues and dark-colored nuclei were easily identifiable on PPF/BMP/hADSCs scaffolds [Fig. 6(G)], whereas nuclei were blue in other groups [Fig. 6(H,I)]. That is to say, HLA-ABC was only revealed on scaffolds using hADSCs. On the PPF/BMP/hADSCs scaffolds, the stained nuclei and cytoplasm around the nuclei of brown color were distributed at the center of the sliced scaffold, and the stained areas occupied a large portion of the whole scaffold. Thus, seeded, differentiated hADSCs were well grown at the inside of the scaffold.

DISCUSSION

Three essential components are required for effective regeneration of target tissue: scaffolds, signals (biomolecules), and cells. In the field of orthopedics, in particular, a scaffold with strong mechanical properties is essential to sustain the pressure and load. The use of a photo-curable biomaterial with strong mechanical properties, such as PPF, enabled the fabrication of scaffolds using the SFF technique. Moreover, the double-emulsion technique makes possible incorporation of the signal in microspheres. In this study, we created a drug-releasing scaffold of high mechanical properties.⁴² BMP-2-loaded microspheres were fabricated using biodegradable PLGA by double-emulsion and solvent-extraction techniques (water-in-oil-in-water), and PPF, which has good mechanical properties, was prepared with a biodegradable photopolymer. Thus, we successfully fabricated the 3D scaffold on which BMP-2-loaded microspheres were presented. As observed on SEM images, all pores of the fabricated MSTL scaffold were perfectly connected, and each strut and pore was fabricated as designed. Furthermore, the distribution of microspheres embedded within the scaffold was uniform.

To observe *in vivo* bone-formation ability, PPF scaffolds, PPF/BMP scaffolds, and PPF/BMP/hADSCs scaffolds were implanted into rat crania. In the rat, hADSCs can cause an immune response. And the purpose of this study was to verify the bone regeneration effect of hADSCs and BMP-2, and the final target was bone regeneration in humans. Therefore, we suppressed the immune response in the rats with an immunosuppressant. Since the bone regeneration at week 11 was pronounced in our previous study, we selected 11 weeks for the animal study and sacrificed the rats by CO₂ inhalation 11 weeks after the surgery.²⁸ After finishing

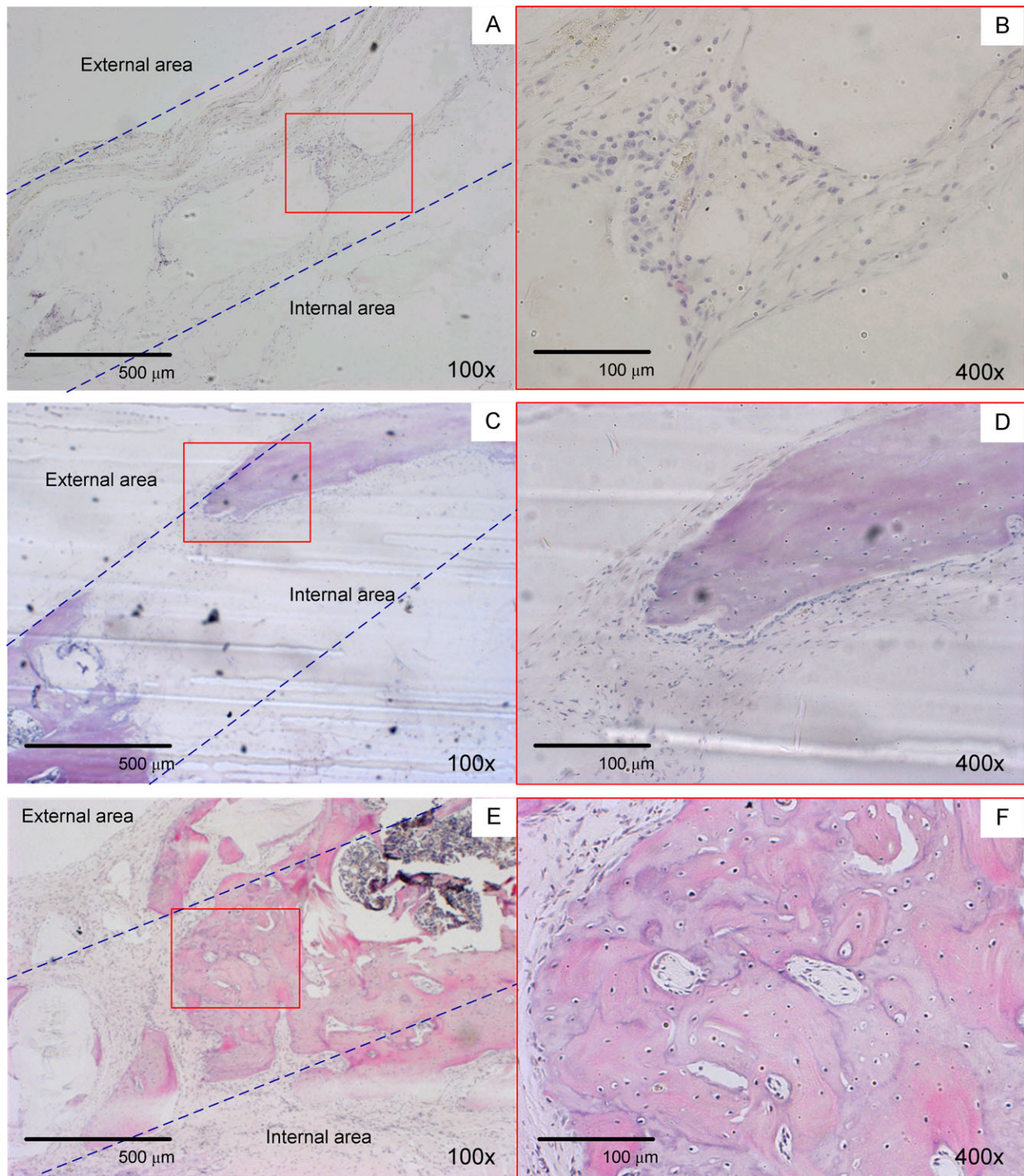


FIGURE 5. Hematoxylin and eosin-stained images (11 weeks after implantation). (A) PPF scaffold (negative control) (100 \times), (B) PPF scaffold (negative control) (400 \times), (C) PPF/BMP scaffold (100 \times), (D) PPF/BMP scaffold (400 \times), (E) PPF/BMP/hADSCs scaffold (100 \times), (F) PPF/BMP/hADSCs scaffold (400 \times). [Color figure can be viewed in the online issue, which is available at wileyonlinelibrary.com.]

the experiment, we measured bone formation areas and the bone-mineral density of the regenerated bone in sacrificed rats. On the PPF/BMP/hADSCs scaffolds, most cranial defects were covered with newly generated bone [Fig. 4(C)]. On the PPF/BMP scaffolds, although bone grew from the

marginal bone toward the inside, the regenerated bone was thinner than that grown on the PPF/BMP/hADSCs scaffolds [Fig. 4(B)]. In the crania repaired with the PPF scaffolds, new bone formed at the edge of original bone, and a small amount of newly formed bone cores was observed near the

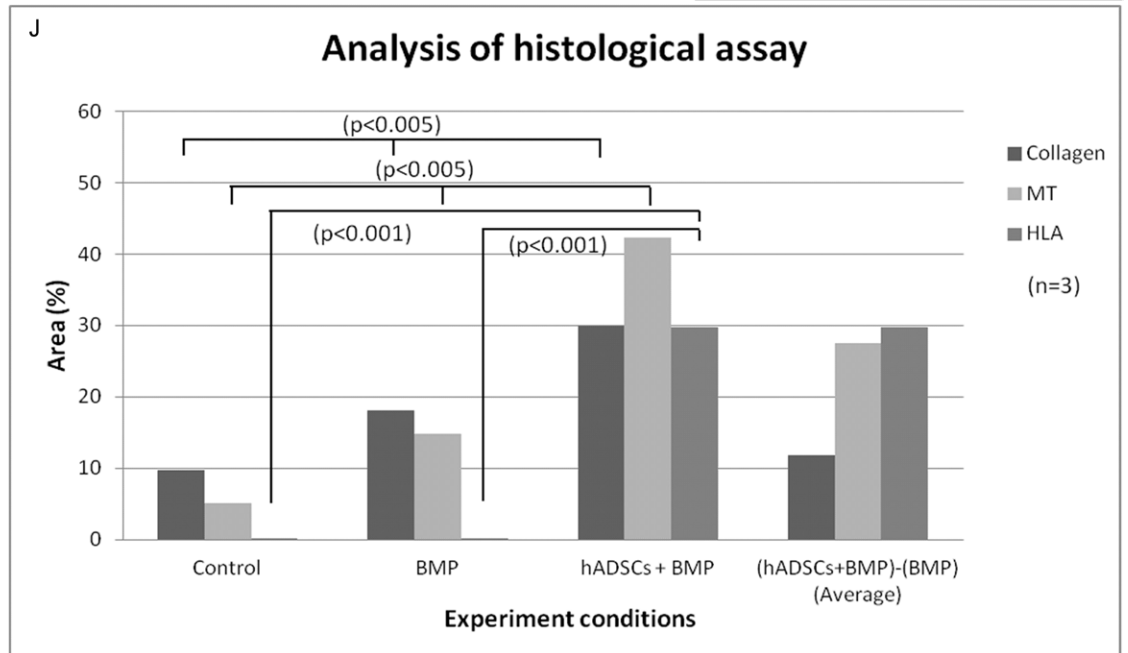
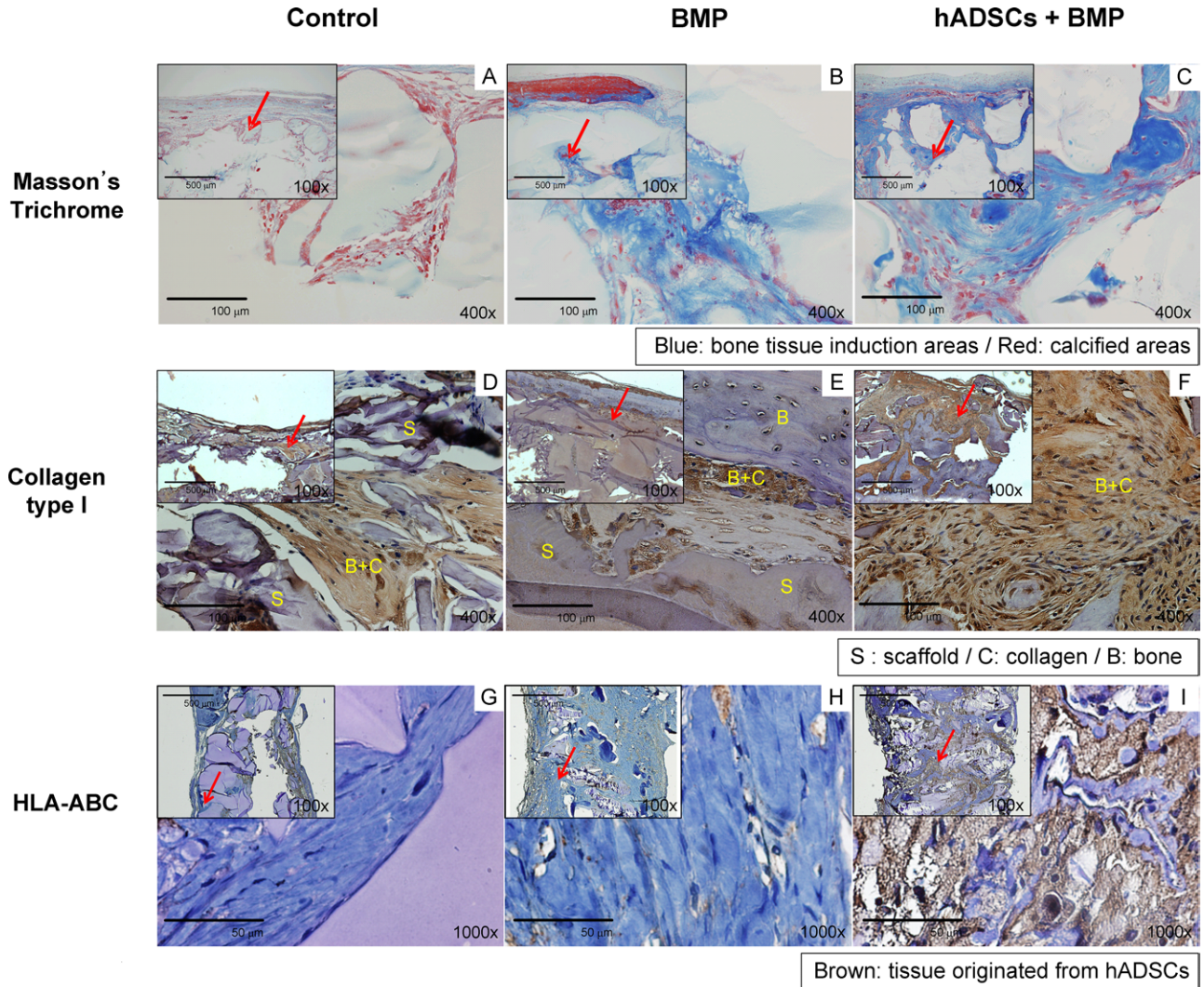


FIGURE 6. Results of histological assay. Masson's Trichrome-stained images (11 weeks after implantation): (A) PPF scaffold (negative control) (100× and 400×), (B) PPF/BMP scaffold (100× and 400×), and (C) PPF/BMP/hADSCs scaffold (100× and 400×). Collagen type-I-stained images (11 weeks after implantation): (D) PPF scaffold (negative control) (100× and 400×), (E) PPF/BMP scaffold (100× and 400×), and (F) PPF/BMP/hADSCs scaffold (100× and 400×). HLA-ABC-stained images (11 weeks after implantation): (G) PPF scaffold (negative control) (100× and 1000×), (H) PPF/BMP scaffold (100× and 1000×), and (I) PPF/BMP/hADSCs scaffold (100× and 1000×). Analysis of stained areas at each condition (J): [scale bar: 500 μm (100×), 100 μm (400×), and 50 μm (1000×)]. [Color figure can be viewed in the online issue, which is available at wileyonlinelibrary.com.]

bone generated at the edge [Fig. 4(A)]. Cross-sectional views of the rat cranium showed the bone-formation results for each group in detail [Fig. 4(D–F)]. The PPF/BMP/hADSCs scaffolds showed thick bone generated at the central part of the defect created by the removed cranial bone. However, on the PPF/BMP scaffolds, the generated bone was thinner than that on the scaffolds using hADSCs. This indicates that hADSCs seeded on the scaffold had changed to bone. Of course, cytokine secretion and ECM deposition that aid actual osteoblast migration and activity facilitated bone growth in this scaffold. In conclusion, bone formation by cells inside the scaffold as well as ingrowth from the outer marginal bones is mandatory to reconstruct sufficient bone tissues. The hADSCs used in this study perfectly performed the role of the cell source for bone regeneration. Moreover, the BMD analysis results were similar to those obtained by micro-CT, and they verified the quality of regenerated bone. The BMD of the bone on the PPF/BMP/hADSCs scaffolds was 50% and 20% denser than that on the PPF scaffolds and PPF/BMP scaffolds, respectively. This result shows that our bone-regeneration tool provided adequate circumstances for cultivating pre-osteoblasts differentiated from hADSCs and that the secreted BMP-2 fostered bone regeneration.

After micro-CT was performed, the implanted scaffolds and their peripheral tissues were extracted from the rats and analyzed using various stain methods. To observe the bone-formation ratio and the effect of hADSCs, we used hematoxylin and eosin stain, Masson's trichrome stain, collagen type-I stain. The results of hematoxylin and eosin staining showed that the new bone was generated and grew from the marginal bone toward the inside of the PPF/BMP scaffolds [Fig. 5(C,D)]. However, on the PPF/BMP/hADSCs scaffolds [Fig. 5(E,F)], newly formed bone and the margin of the original bone were fused throughout the scaffold from the edge to the center of the scaffold. The greatest bone reconstruction clearly occurred in this group. Several parts of the scaffold structure were entrapped and degraded within the new bone. Both Masson's trichrome stain [Fig. 6(A–C)] and collagen type-I stain [Fig. 6(D–F)] showed that BMP-2, which was secreted by our functional scaffold, induced bone formation from the outer marginal bone, and hADSCs seeded in the scaffold generated a new bone on the scaffold at the interior of the defect. In conclusion, synergy between BMP-2 and hADSCs resulted in the regeneration of bone from the outside edge of the defect to the center of the scaffold.

One aim of this study was to confirm the role of the cell, which is an essential component of tissue regeneration. For such confirmation, it is required that actual bone was formed from hADSCs. Comparisons of CT images of PPF/BMP/hADSCs and PPF/BMP scaffolds demonstrated the role of hADSCs by showing the existence of thick bone generated at the central part of the cranial defect. By identifying the origin of each area of regenerated bone, we could validate the effect of hADSCs. We confirmed the presence of HLA-ABC, which is detected only in human cells and extra cellular matrix (ECM). The results of the HLA-ABC stain revealed

brown-stained ECM only on the PPF/BMP/hADSCs scaffolds [Fig. 6(G–I)]. That is, the center zone of this sample was composed of human-cell-derived tissue.

Histological assay results were similar to the findings from micro-CT. Secreted BMP-2 from the scaffold promoted the bone ingrowth from outside the scaffold, and pre-osteoblasts differentiated from hADSCs adhered to inside of the scaffold, generating a new bone and extending the ossified areas. By these activities, the PPF/BMP/hADSCs scaffolds demonstrated powerful bone-formation ability [Fig. 6(J)]. From this study, we confirmed that collaboration among scaffolds, cells, and biomolecules is essential to regenerate sufficient bones.

CONCLUSIONS

In this report, we proposed a novel bone-tissue-regeneration tool using hADSCs and a 3D scaffold-embedded with signal-deliverable carrier. Thus, using PLGA microspheres containing BMP-2, a 3D scaffold was fabricated with PPF/DEF, which has high mechanical properties by MSTL. And hADSCs gathered from fat extracted using liposuction were seeded at the developed scaffold. Then, we assessed the bone-formation ability of this system in an animal model. The bone formation results using Micro-CT and histological assays of the resulting bone formation showed that our combination of a functional 3D scaffold and hADSCs may be a useful tool for improving the reconstruction quality of actual bony defects in which thick bone is required. Furthermore, because our SFF-based technology can supply a customized 3D scaffold, we anticipate that it will show a powerful ability to repair complex bony defects that require 3D reconstruction.

REFERENCES

1. Barrilleaux B, Phinney DG, Prockop DJ, O'Connor KC. Review: *Ex vivo* engineering of living tissues with adult stem cells. *Tissue Eng* 2006;12:3007–3019.
2. Kim MH, Hong HN, Hong JP, Park CJ, Kwon SW, Kim SH, Kang G, Kim M. The effect of VEGF on the myogenic differentiation of adipose tissue derived stem cells within thermosensitive hydrogel matrices. *Biomaterials* 2010;31:1213–1218.
3. Cui L, Liu B, Liu G, Zhang W, Cen L, Sun J, Yin S, Liu W, Cao Y. Repair of cranial bone defects with adipose derived stem cells and coral scaffold in a canine model. *Biomaterials* 2007;28: 5477–5486.
4. Zuk PA, Zhu M, Mizuno H, Huang J, Futrell JW, Katz AJ, Benhaim P, Lorenz HP, Hedrick MH. Multilineage cells from human adipose tissue: Implications for cell-based therapies. *Tissue Eng* 2001;7: 211–228.
5. Zuk PA, Zhu M, Ashjian P, De Ugarte DA, Huang JI, Mizuno H, Alfonso ZC, Fraser JK, Benhaim P, Hedrick MH. Human adipose tissue is a source of multipotent stem cells. *Mol Biol Cell* 2002;13: 4279–4295.
6. De Ugarte DA, Morizono K, Elbarbary A, Alfonso Z, Zuk PA, Zhu M, Dragoo JL, Ashjian P, Thomas B, Benhaim P, Chen I, Fraser J, Hedrick MH. Comparison of multi-lineage cells from human adipose tissue and bone marrow. *Cells Tissues Organs* 2003;174: 101–109.
7. Fernyhough ME, Hausman GJ, Guan LL, Okine E, Moore SS, Dodson MV. Mature adipocytes may be a source of stem cells for tissue engineering. *Biochem Biophys Res Co* 2008;368:455–457.
8. Wu KH, Mo XM, Liu YL, Zhang YS, Han ZC. Stem cells for tissue engineering of myocardial constructs. *Ageing Res Rev* 2007;6: 289–301.

9. Wu KH, Liu YL, Zhou B, Han ZC. Application of stem cells for cardiovascular grafts tissue engineering. *Transpl Immunol* 2006;16:1-7.
10. Thomson R, Yaszemski M, Mikos AG. Polymer scaffold processing. In: Lanza R, Langer R, Chick W, editors. *Principles of Tissue Engineering*. Texas: R.G. Landes Co.;1997. p263-272.
11. Agrawal CM, Athansiou KA, Heckman JD. Biodegradable PLGA polymers for tissue engineering in orthopaedics. *Mater Sci Forum* 1997;250:115-128.
12. Langer RB. Selected advances in drug delivery and tissue engineering. *J Control Release* 1999;62:7-11.
13. Lu L, Mikos AG. The importance of new processing techniques in tissue engineering. *MRS Bull* 1996;21:28-32.
14. Mikos AG, Thorsen AJ, Czerwonka LA, Bao Y, Langer RB. Preparation and characterization of poly (l-lactic acid) forms. *Polymer* 1994;35:1068-1077.
15. Mikos AG, Bao Y, Cima LG, Ingeber DE, Vacanti JP, Langer RB. Preparation of poly (glycolic acid) bonded fiber structures for cell attachment and transplantation. *J Biomed Mater Res* 1993;27:183-189.
16. Mikos AG, Sarakinos G, Leite SM, Vacanti JP, Langer RB. Laminated three-dimensional biodegradable foams for use in tissue engineering. *Biomaterials* 1993;14:323-330.
17. Mooney DJ, Baldwin DF, Suh NP, Vacanti JP. Novel approach to fabricate porous sponges of poly (D, L-lactic-co-glycolic acid) without the use of organic solvents. *Biomaterials* 1996;17:1417-1422.
18. Zein I, Huttmacher DW, Tan KC, Teoh SH. Fused deposition modeling of novel scaffold architectures for tissue engineering applications. *Biomaterials* 2002;23:1169-1185.
19. Dutt RT, Simon JL, Ricci JL, Rekow ED, Thompson VP, Parsons JR. Performance of hydroxyapatite bone repair scaffolds created via three-dimensional fabrication techniques. *J Biomed Mater Res A* 2003;67:1228-1237.
20. Chu TM, Orton DG, Hollister SJ, Feinberg SE, Halloran JW. Mechanical and *in vivo* performance of hydroxyapatite implants with controlled architectures. *Biomaterials* 2002;23:1283-1293.
21. Gratson GM, Xu M, Lewis JA. Direct writing of three dimensional webs. *Nature* 2004;428:386.
22. Barry III RA, Shepherd RF, Hanson JN, Nuzzo RG, Wiltzius P, Lewis JA. Direct-write assembly of 3D hydrogel scaffolds for guided cell growth. *Adv Mater* 2009;21:2407-2410.
23. Kodama H. Automatic method for fabricating a three-dimensional plastic model with photo-hardening polymer. *Rev Sci Instrum* 1981;52:1770-1773.
24. Cooke MN, Fisher JP, Dean D, Rimnac C, Mikos AG. Use of stereolithography to manufacture critical-sized 3D biodegradable scaffolds for bone ingrowth. *J Biomed Mater Res B* 2002;64:65-69.
25. Lee JW, Lan PX, Kim B, Lim G, Cho D-W. Fabrication and characteristic analysis of a poly (propylene fumarate) scaffold using micro-stereolithography technology. *J Biomed Mater Res B* 2008;87:1-9.
26. Kim J, Lim D, Kim YH, Koh Y-H, Lee MH, Han I, Lee SJ, Yoo OS, Kim H-S, Park J-C. A comparative study of the physical and mechanical properties of porous hydroxyapatite scaffolds fabricated by solid freeform fabrication and polymer replication method. *IJPEM* 2011;12:695-701.
27. Kwon IK, Matsuda T. Photo-polymerized microarchitectural constructs prepared by microstereolithography using liquid acrylated-end-capped trimethylene carbonate-based prepolymers. *Biomaterials* 2005;26:1675-1684.
28. Lee JW, Kang KS, Lee SH, Kim J-Y, Lee B-K, Cho D-W. Bone regeneration using a microstereolithography-produced customized poly(propylene fumarate)/diethyl fumarate photopolymer 3D scaffold incorporating BMP-2 loaded PLGA microspheres. *Biomaterials* 2011;32:744-752.
29. Kim JY, Jin G-Z, Park IS, Kim J-N, Chun SY, Park EK, Kim S-Y, Yoo JY, Kim S-H, Rhie J-W, Cho D-W. Evaluation of SFF-based scaffolds seeded with osteoblasts and HUVECs for use *in vivo* osteogenesis. *Tissue Eng Part A* 2010;16:2229-2236.
30. Jung JW, Kang H-W, Kang T-Y, Park JH, Park J, Cho D-W. Projection image-generation algorithm for fabrication of a complex structure using projection-based microstereolithography. *IJPEM* 2012;13:445-449.
31. Tabata Y. Tissue regeneration based on growth factor release. *Tissue Eng* 2003;9:S5-S15.
32. Aebischer P, Salessiotis AN, Winn SR. Basic fibroblast growth factor released from synthetic guidance channels facilitates peripheral nerve regeneration across long nerve gaps. *J Neurosci Res* 1989;23:282-289.
33. Arm DM, Tencer AF, Bain SD, Celino D. Effect of controlled release of platelet-derived growth factor from a porous hydroxyapatite implant on bone in growth. *Biomaterials* 1996;17:703-709.
34. DeBlois C, Cote MF, Doillon CJ. Heparin-fibroblast growth factor-fibrin complex: *In vitro* and *in vivo* applications to collagen-based materials. *Biomaterials* 1994;15:665-672.
35. Heckman JD, Boyan BD, Aufdemorte TB, Abbott JT. The use of bone morphogenetic protein in the treatment of non-union in a canine model. *J Bone Joint Surg Am* 1991;73:750-764.
36. Hong L, Tabata Y, Yamamoto M, Miyamoto S, Yamada K, Hashimoto N, Ikada Y. Comparison of bone regeneration in a rabbit skull defect by recombinant human BMP-2 embedded in biodegradable hydrogel and in solution. *J Biomater Sci: Polym Ed* 1998;9:1001-1014.
37. Lee M, Chen TT, Iruela-Arispe ML, Wu BM, Dunn JC. Modulation of protein delivery from modular polymer scaffolds. *Biomaterials* 2007;28(10):1862-1870.
38. Ko EK, Jeong SI, Rim NG, Lee YM, Shin H, Lee B-K. *In vitro* osteogenic differentiation of human mesenchymal stem cells and *in vivo* bone formation in composite nanofiber meshes. *Tissue Eng Part A* 2008;14:2105-2119.
39. Chen D, Harris MA, Rossini G, Dunstan CR, Dallas SL, Feng JQ, Mundy GR, Harris SE. Bone morphogenetic protein 2 (BMP-2) enhances BMP-3, BMP-4, and bone cell differentiation marker gene expression during the induction of mineralized one matrix formation in cultures of fetal rat calvarial osteoblasts. *Calcif Tissue Int* 1997;60:283-290.
40. Yamaguchi A, Ishizuya T, Kintou N, Wada Y, Katagiri T, Wozney JM, Rosen V, Yoshiki S. Effects of BMP-2, BMP-4, and BMP-6 on osteoblastic differentiation of bone marrow-derived stromal cell lines, ST2 and MC3T3-G2/PA6. *Biochem Biophys Res Commun* 1996;220:366-371.
41. Ji X, Chen D, Xu C, Harris SE, Mundy GR, and Yoneda T. Patterns of gene expression associated with BMP-2 induced osteoblast and adipocyte differentiation of mesenchymal progenitor cell 3T3-F442A. *J Bone Miner Metab* 2000;18:132-139.
42. Lee JW, Ahn G, Kim J.Y, Cho D-W. Evaluation of cell proliferation and differentiation on a poly (propylene fumarate) 3D scaffold treated with functional peptides. *J Mater Sci: Mater Med* 2010;21:3195-3205.